A study on multiscale wavelet analysis in recognizing earthquake-induced signals in the medium-to-short wavelength part

Sang-Hoon Park, Seok-Woo Hong

Abstract: ***Mw 9.0 Tohoku-Oki earthquake occurred in the sedimentary area between the Pacific and North American tectonic plates on March 11, 2011. There is no record of a magnitude 9.0 earthquake along Japan Trench except the Jogan earthquake on July 13, AD 869, which may be the only documented incident of similar magnitude and location to the Tohoku-Oki earthquake. Since large crustal deformations indicate mass redistribution within the solid Earth, an earthquake also affects the gravitational field that has the temporal variations reflecting the mass redistribution inside the solid Earth processes. In general, it is difficult to isolate the earthquake anomalies from other signals in the frequency domain since frequencies change spatially due to the contribution of a certain combination of frequencies and this spatial rise of the frequencies is not reflected in the spherical harmonics. In this study, the researchers use monthly GRACE gravity data and apply the multiscale wavelet analysis, based on the Abel-Poisson scale and its corresponding wavelet functions to monthly GRACE gravity data in order to extract the Tohoku-Oki earthquake-induced signals in the medium-to-short-wavelength part. As a result of this largest earthquake, there was some coseismic mass redistribution producing local geoid changes. In March 2011, the coseismic geoid decrease was detected at the northwestern part of Yamagata Prefecture, which increased consistently until February 2011. With regard to the postseismic geoid recovery, changes at the eastern part of northern Honshu near the Miyagi segment and the southern part of the Sanriku segment near the Japan Trench were predominant in August 2011. It is concluded that the geological relationship among these locations played a very important role in the Tohoku-Oki earthquake occurrence. Furthermore, the tectonic plate motion around the Japanese islands may reach a period of geological stability after August 2011.***

Keywords: Abel-Poisson wavelet function; GRACE observation; Multiscale wavelet analysis; Seismic geoid variation; Tohoku-Oki earthquake

I. INTRODUCTION

The Japanese is located at the intersection of the Pacific Ocean, North American, Philippine Sea and Eurasian plates. On March 11, 2011 the Tohoku-Oki earthquake, with a magnitude of 9.0, occurred in the sedimentary area between the Pacific and North American tectonic plates. And the Pacific Plate goes westward underneath the North American Plate at a rate of ~80 mm·yr^{-1} relative to the Eurasian [1]. The earthquake is recorded as the fourth-largest one in the world during the last century.Most major earthquakes occur along oceanic trenches where the oceanic plate sinks below the continental plate. Historically, many Mw 7 to Mw 8 earthquakes such as Tokachi, Sanriku, Miyagi, and Fukushima have occurred in Japan Trench [2]. However, there is no record of a magnitude 9.0 earthquake along Japan Trench except the Jogan earthquake on July 13, AD 869, which may be the only documented incident of similar magnitude and location to the Tohoku-Oki earthquake [3]. Earth gravity field modeling that always governed by the classical Newtonian law has the temporal variations reflecting the mass redistribution inside the solid Earth at different spatial and time-scales. Besides the primary contribution by solid Earth tides, mass redistribution occurs at daily, semi-annual and annual, inter-annual, secular, etc. They largely mirror water redistribution between various sources such as the atmosphere, land hydrological systems, oceans and arctic ice caps. This phenomenon leads to significant seasonal changes of up to several millimeters above the geoid height on a global scale [4].Earthquakes can result in large crustal deformations in the order of a few meters of uplift or subsidence. Since these deformations imply mass redistribution within the solid Earth, an earthquake also affects the gravitational field that has the temporal variations reflecting the mass redistribution inside the solid Earth processes [5]. On shorter time and spatial scales, redistribution of masses by largest earthquake causes local variations of the geoid to few [4].In the past, Satellite Laser Ranging (SLR) has been used to determine the very long wavelength seasonal gravity changes due to the interchange of mass between the atmosphere, ocean, and continental water. And measurements obtained from SLR have been limited in resolution because of the geographic distribution of the tracking data and the high altitude of the satellites.However, this situation has changed after the launch of the Gravity Recovery And Climate Experiment (GRACE) satellite in 2002. GRACE satellite gravity mission accomplishes global measurements of the gravity field and its time change with a high precision and uniform coverage. Monthly time-series of the gravity field from the GRACE data, in the form of spherical harmonic coefficients, have been producing indispensable implications and insights about large scale terrestrial water, ocean, ice sheet, fast and slow deformations of the solid Earth such as earthquake and postglacial rebound. Also GRACE data sets include coseismic deformation reflecting the redistribution of mass because geophysical effects have already been eliminated by modeling [6], [7], [8], [9].The expansion of spherical harmonics is fundamental to studying the various components of the gravity field that can be determined by the derivatives of the geopotential function every month, and the time-variable changes for the satellite gravity can be examined based on these data. The accuracy relies on that of the spherical harmonic coefficients (C_{lm} and S_{lm}) and the spatial resolution, where l and m are the degree and order of the spherical harmonic coefficients respectively, whereas the spatial resolution is determined by the maximum degree l_{max}, the larger the l_{max}, the higher the spatial resolution.

Revised Manuscript Received on May 06, 2019

Sang-Hoon Park, Department of Civil Engineering, Dong-eui University, Busan, South Korea

Seok-Woo Hong, Department of Civil Engineering, Dong-eui University, Busan, South Korea

At present, noise, as proven by longitudinal stripes on gravity field, dominates the high degree and order spherical harmonics of the GRACE gravity data. Due to the attenuation of signals, the GRACE satellite become known to measure only low-frequency gravity. In practical applications of satellite gravity data, a filter is usually used for reducing the error in the high-frequency part of the signal. In recent years, many researchers studying in satellite gravity techniques and applications have developed different filtering methods such as non-isotropic Gaussian filtering [10], optimized filtering [11], Gaussian filtering and decorrelation [12], Wienner optimal filtering [13], fan filtering [14] and wavelet analysis methods [15] in order to obtain better spatial resolutions and identify signals of localized deformations [16].

Several studies have been investigated the earthquake-induced signals in the GRACE-derived gravity data. For example, the coseismic gravity changes associated with the Tokachi-Oki earthquake in 2003 were identified by using gravimetry [17]. Furthermore, according to Sun and Okubo [18], the GRACE mission theoretically is able to decide the coseismic gravity changes arisen from an earthquake with magnitude of 8 or greater. Subsequently, the coseismic and postseismic gravity changes caused by 2004 Sumatra-Andaman earthquake with magnitude 9.3 were dented by the GRACE [8], [16], [19], [20]. Recently, the coseismic gravity changed due to the Chile earthquake in 2010 with magnitude 8.8 were investigated by the GRACE gravity data [21], [22].

In this study, the researchers use 25 GRACE L2 Release 04 monthly gravity data from GeoForschungsZentrum (GFZ) covering the period from January 2010 to March 2012 with the exception of January 2011 as well as June 2011 and apply the multiscale wavelet analysis using the Abel-Poisson scale and its corresponding wavelet functions as described in [15], [23], [24], [25], to GRACE Level 2 Release 04 gravitational data for individual point of a 0.1°×0.2° grid space in order to extract the Tohoku-Oki earthquake-related signals in the medium-to-short-wavelength part. Any post-processing is not applied to eliminate the high frequency 'longitudinal-stripe' errors in GRACE gravitational solutions, since de-striping or decorrelation not only removes errors but also eliminates seismic gravity change signals that occur near the longitudinal patterns or stripes before reconstructing our multiscale geoid models. Also, we replaced the zonal harmonic terms such as C_{20}, C_{40} and C_{60} with those from GRS80 in order to obtain more accurate geoid models when calculating coefficients. Then, the Tohoku-Oki earthquake-induced signals are detected and investigated. Finally, the coseismic and postseismic changes in the geoid anomalies, as evidenced by the wavelet analysis, are analyzed and discussed.

II. Data processing

2.1. GRACE mission

Lately combined gravity models of mean gravity values, information from satellite radar altimetry, and orbit analysis of satellites have been used. However, these three data sources cannot be satisfied with the requirements from Earth physics, oceanography, physical geodesy, etc. The traditional techniques of Earth's gravitational field determination are faced with intrinsic limitations in their accuracy and resolution since an orbit is somewhat less sensitive to the local characteristics of the gravitational field in order to detect short-wave phenomena. Therefore, space techniques are needed to provide global, regular, and dense datasets of high and homogeneous quality

The GRACE mission is a joint project between the U.S. National Aeronautics and Space Administration (NASA) and the Deutsches Zentrum für Luft und Raumfahrt (DLR). The main objectives are the global high-resolution gravity field determination of the earth. Two satellites of this mission were launched on March 17, 2002 with (eccentricity $e <$ 0.005) and near-polar orbit (inclination angle = 89°). The altitude of the GRACE satellites between 485 km and 500 km decreases in the course of their lifetime because of atmospheric drag. The range between the two satellites must be determined accurately since variations in the gravity field cause variations in the range between the two satellites. Its range rate is measured by intersatellite microwave measurements.

The measuring principle for GRACE is satellite-to-satellite tracking (SST) in low-low mode shown in Fig. 1. Two LEO satellites are in the same orbit but separated by about 220 km. Ranges and range rates between the satellites are achieved to maximum accuracy. In addition, GPS satellites determine the position of the LEOs. The effect of non-gravitational forces on the satellite due to air drag must be calibrated with an accelerometer. In 2004, the GRACE team released a first version of an earth gravity model up to degree and order 150.

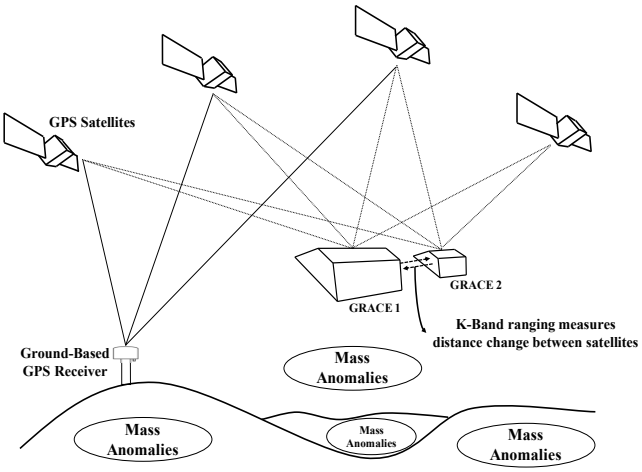

Fig. 1: GRACE satellite and its measuring principle

2.2. Geopotential model

The knowledge based on potential theory is important to any science that contribute to the study of a planetary system like the Earth. Starting from simple ellipsoidal normal gravity models to complex high degree spherical harmonics, a geopotential model representing the Earth's gravity or gravitational potential and/or gravity values has been developed and estimated in this century. Once it was conceptualized that the Earth's gravitational field could be determined by methods of classical potential theory as a solution to the outer boundary value problem. Until now unrealistic assumption of boundary data that the Earth's actual surface does not match an equipotential surface of the gravity field was required in geodetic and geophysical applications.

According to Heiskanen and Moritz [26], the potential of gravitational attraction between a unit mass and the Earth system is represented by using an infinite spherical harmonic series as pointed in (1). The point is specified by its geocentric radius r, geographic latitude θ, and longitude λ. If GM and a_e represent the gravitational constant of the Earth and mean equatorial radius, respectively, then the Earth's outer potential can be represented as

$$V = \frac{GM}{r}\left(1 + \sum_{n=1}^{\infty}\sum_{m=0}^{n}\left(\frac{a_e}{r}\right)(\bar{C}_{nm}\cos m\lambda + \bar{S}_{nm}\sin m\lambda)\bar{P}_{nm}(\cos\theta)\right) \quad (1)$$

where $\bar{P}_{nm}(\cos\theta)$ are the fully-normalized Associated Legendre Polynomials of degree n and order m, $\bar{C}_{nm}$ and $\bar{S}_{nm}$ are the spherical harmonic coefficients of the geopotential.
The geopotential at a fixed location is variable in time due to mass distribution and exchange between the Earth system components. Through an infinite series of harmonics is actually required, the summation on the right-hand side of equation (1) can be practically limited to a maximum degree $n_{\max}$. In satellite geodetic convention, the origin of the reference coordinate frame is chosen to be matched with the mass center of the entire Earth system, including its solid component and fluid envelopes. Therefore the potential does not have terms of degree n=1 on the right-hand side of equation (1).In the past, the determination of the earth's geopotential model is restricted to the spherical harmonic expansion to low degree because the terrestrial data coverage remained poor. However, many types of observation are nowadays available, including terrestrial gravimetry, airborne gravimetry, satellite-to-satellite tracking, satellite gradiometry, etc. So all updated global geopotential models include orthogonal coefficients up to the $n \geq 360$.
These days the use of spherical harmonics is a well-established technique in physical geodesy for representing globally geopotentials on the earth surface given by tables of coefficients for the spherical harmonic expansion such as GRIM4-S4, EGM84, EGM96, EGM08, EIGEN-GRACE01S, GGM01S, etc. [23], [24], [42].

2.3. Multiscale wavelet analysis

Generally, global long-wavelength approximation can be adequately performed by Fourier expansions in terms of spherical harmonics. However, it cannot provide more information for the part of medium- and short-wavelength approximation equivalent to the high degree of spherical harmonic expansion, associated with geophysical signals such as tides, atmosphere and earthquakes, etc., because it includes the total amplitude of the frequency instead of distribution of the harmonic modes at each individual location.
For over two centuries spherical approximation by Fourier expansions has been used for analyzing geophysical quantities. But this approach is not applied efficiently and economically to the excessive regional change of the density in data points and the enormous amount of satellite observations requiring trial functions with the spherical harmonics.
In consequence, local variations of a geophysical signal caused by movement of the earth's crust ask an entirely new calculation in a Fourier expansion with the help of trial functions with the spherical harmonics. Also, Fourier transform can only reflect the frequency property of signal. So kernel functions localizing sufficiently well in space domain as well as in frequency domain is needed. The trade-off between space localization on the sphere and frequency localization in terms of kernel functions is described in form of an uncertainty principle based on the variance that is the chief measure for a function defined on Euclidean space. In order to overcome these restrictions, spherical wavelets are introduced by which the gravitational part of the gravity field can be approximated progressively better and better [27], [29], [30], [31].
Spherical wavelets are used as mathematical tool for breaking up a complicated structure of a function into many simple pieces at different scales and positions. And a multiscale wavelet analysis based on Spherical wavelet functions enables a balanced amount of both frequency and space localization since spherical wavelets show well-adapted properties of space and frequency localization [24], [28], [32], [33], [34].
By virtue of the Bruns formula $N = T/r$, J-level representation of the geoid undulations on the sphere Ω_R can be written in terms of a low-frequency band and wavelet. Also, it can be computed from the multiscale decomposition of the distribution potential. Therefore, the multiscale geoid height, N, are described in (2).

$$N_J(x) = \int_{\Omega_R}\Phi_{j_0}(x,y)\int_{\Omega_R}\Phi_{j_0}(z,y)N(z)d\omega(z)\,d\omega(y) + \sum_{j=j_0}^{J-1}\int_{\Omega_R}\widetilde{\Psi}_j(x,y)\int_{\Omega_R}\Psi_j(z,y)N(z)d\omega(z)\,d\omega(y)$$

$$\approx \sum_{i=1}^{(N_{j_0}+1)^2}\omega_i^{j_0}\,a_i^{j_0}\,\Phi_{j_0}\left(x,y_i^{j_0}\right) + \sum_{j=j_0}^{J-1}\sum_{i=1}^{(N_j+1)^2}\omega_i^{j}\,c_i^{j}\,\widetilde{\Psi}_j\left(x,y_i^{j}\right) \quad (2)$$

where $\left(y_i^{j_0},\omega_i^{j_0}\right)$ and $\left(y_i^{j},\omega_i^{j}\right)$ are the locations on the sphere Ω_R and corresponding integration weights of the Driscoll-Healy integration scheme for the different parameters N_{j_0} and N_j to integrate bandlimited functions, $a_i^{j_0}$ and c_i^{j}, as pointed in (3), are the scaling and wavelet coefficients obtained by numerical integration using an equiangular grid as presented by Driscoll and Healy [35], Φ_j is the kernel in terms of scaling function, and Ψ_j and $\widetilde{\Psi}_j$ are kernels of the corresponding j-th the primal and dual wavelets, as represented in (4), (5) and (6) respectively.

$$a_i^{j_0} = \int_{\Omega_R} \Phi_{j_0}(z, y_i^{j_0}) N(z)\, d\omega(z) \approx \sum_{k=1}^{(\tilde{N}_{j_0}+1)^2} \tilde{\omega}_k^{j_0}\, \Phi_{j_0}(\tilde{z}_k^{j_0}, y_i^{j_0})\, N(\tilde{z}_k^{j_0})$$

$$c_i^j = \int_{\Omega_R} \Psi_j(z, y_i^j) N(z)\, d\omega(z) \approx \sum_{k=1}^{(\tilde{N}_j+1)^2} \tilde{\omega}_k^j\, \Psi_j(\tilde{z}_k^j, y_i^j)\, N(\tilde{z}_k^j) \qquad (3)$$

where $(\tilde{z}_k^{j_0}, \tilde{\omega}_i^{j_0})$ and $(\tilde{z}_k^j, \tilde{\omega}_i^j)$ denote the points and weights of the integration formula that has to be chosen such that it integrates bandlimited functions exactly up to degree $\tilde{N}_{j_0}$ or $\tilde{N}_j$, respectively.

For the Abel-Poisson scaling function, the following is taken:

$$\varphi_j^{AP}(n) = e^{-2^{-j}\alpha n}, \qquad \alpha > 0.$$

Then the Abel-Poisson scaling function can be represented by a sum over Legendre polynomials [36]

$$\Phi_j^{AP}(x,y) = \sum_{n=0}^{\infty} \frac{2n+1}{4\pi R^2} \varphi_j^{AP}(n) P_n\left(\frac{x}{|x|}\cdot\frac{y}{|y|}\right) = \frac{1}{4\pi R^2} \frac{1 - e^{-2^{-j+1}}}{\left(1 + e^{-2^{-j+1}} - 2e^{-2^{-j}} t\right)^{\frac{3}{2}}} \qquad (4)$$

where α=1 and $t = \frac{x}{|x|}\cdot\frac{y}{|y|}$.

By using M-scale wavelets, the primal and dual wavelets can be written as follow:

$$\Psi_j^{AP}(x,y) = \sum_{n=0}^{\infty} \frac{2n+1}{4\pi R^2} \psi_j^{AP}(n) P_n\left(\frac{x}{|x|}\cdot\frac{y}{|y|}\right) = \Phi_{j+1}^{AP}(x,y) - \Phi_j^{AP}(x,y) \qquad (5)$$

$$\tilde{\Psi}_j^{AP}(x,y) = \sum_{n=0}^{\infty} \frac{2n+1}{4\pi R^2} \tilde{\psi}_j^{AP}(n) P_n\left(\frac{x}{|x|}\cdot\frac{y}{|y|}\right) = \Phi_{j+1}^{AP}(x,y) + \Phi_j^{AP}(x,y) \qquad (6)$$

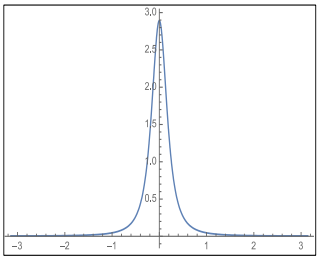

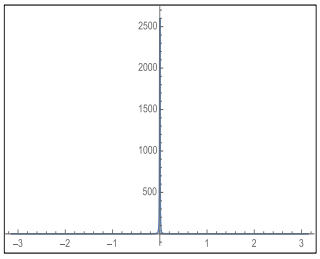

Fig. 2: Space localization by Abel-Poisson scaling function at scale 2(left) and scale 7 (right)

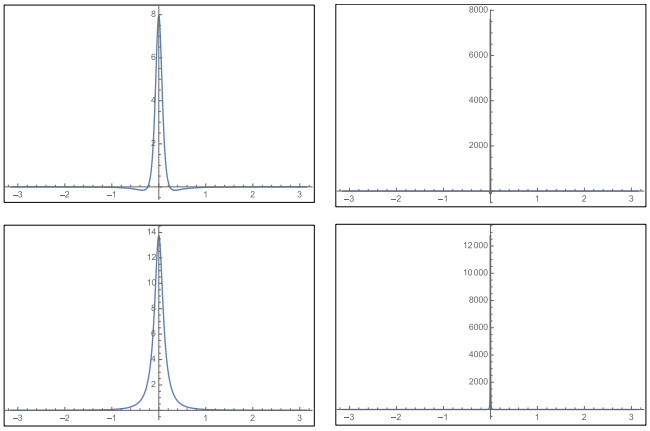

Fig. 3: Space localization by Abel-Poisson wavelet (top: the primal wavelet, bottom: the dual wavelet) at scale 2(left) and scale 7 (right)

Since the Abel-Poisson scaling function and its corresponding wavelets are non-bandlimited, an exact integration can be obtained via the numerical integration method, based on an equiangular grid.

Figure 2 and Figure 3 present the property that shows space localization by Abel-Poisson scaling function, the primal and the dual wavelets, respectively. Reconstruction of GRACE gravity data using the multiscale wavelet analysis on the sphere is described more specifically in [23], [30].

III. Results

3.1. Monthly geoid model vs multiscale geoid model

Figure 4 presents the monthly geoid models observed by GRACE for February 2011, March 2011, and April 2011. Although the difference between February 2011 and March 2011 shows range -0.30723~0.35266, the researchers cannot clearly identify that those differences among geoid models come from the Tohoku-Oki earthquake.

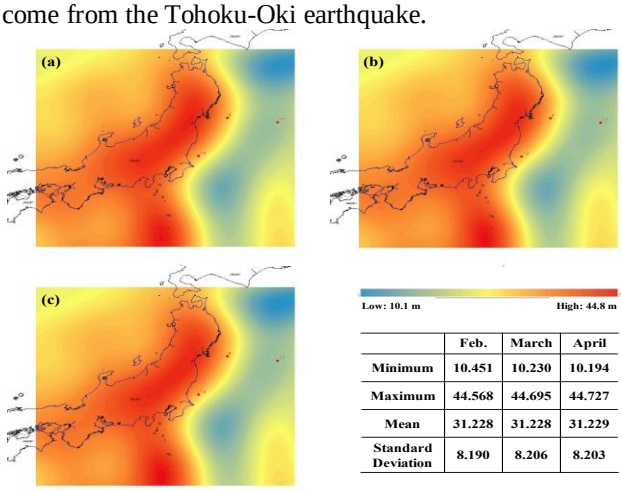

	Feb.	March	April
Minimum	10.451	10.230	10.194
Maximum	44.568	44.695	44.727
Mean	31.228	31.228	31.229
Standard Deviation	8.190	8.206	8.203

Fig. 4: Monthly geoid models observed by GRACE on individual points of a 0.1°×0.2° grid space for (a) February 2011, (b) March 2011, and (c) April 2011. (unit: meter)

Figure 5 shows the box plots in a series into the median, the upper and lower quartiles, and the minimum and maximum values showing center, spread, range, and any outliers with respect to monthly geoid models observed by GRACE and shows the same result as Fig. 4.

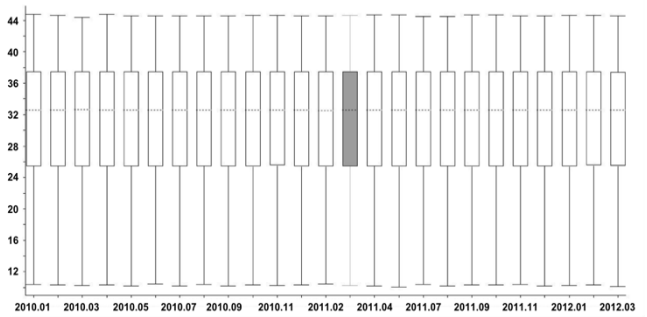

Fig. 5: Time-series of box plot with respect to monthly geoid models for the period from January 2010 to March 2012. Mean geoid value for the whole period is 31.23148 m with range 10.28595~44.61724 m and standard deviation 8.19931 m. (unit: meter)

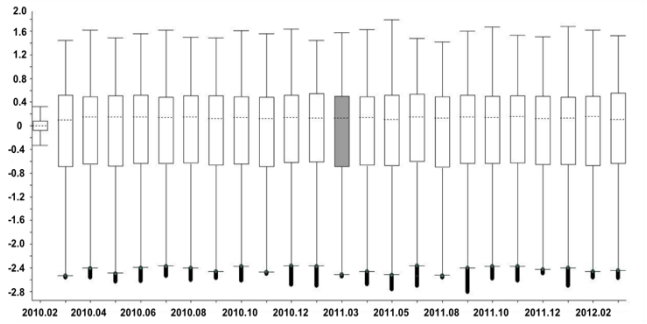

Fig. 6: Time-series of box plot with respect to the differences between monthly geoid models from February 2010 to May 2011 and that of January 2010 selected as the reference. (unit: meter)

In order to provide a more detailed investigation on the coseismic geoid changes, monthly geoid model for January 2010 was selected as the reference for comparison, and those from February 2010 to March 2012 is differenced with this reference.

As shown in Fig. 6, any significant geoid changes arisen from the Tohoku-Oki earthquake cannot be found in terms of the pattern just except showing the small differences in the order a few tenths of centimeters in terms of center, spread and range of each geoid model.

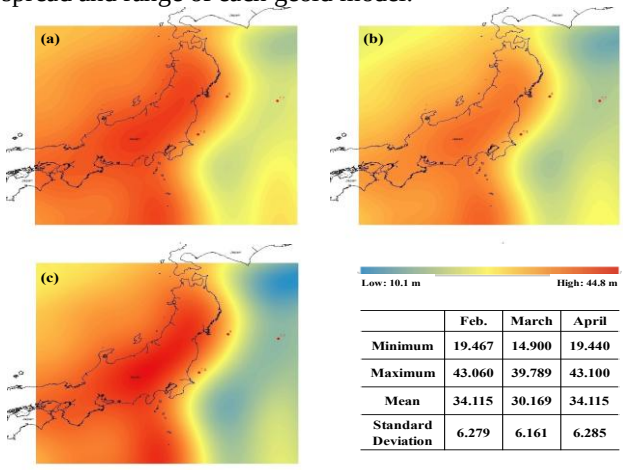

	Feb.	March	April
Minimum	19.467	14.900	19.440
Maximum	43.060	39.789	43.100
Mean	34.115	30.169	34.115
Standard Deviation	6.279	6.161	6.285

Fig. 7.: Multiscale geoid models based on the GRACE gravity data on individual points of a 0.1°×0.2° grid space for (a) February 2011, (b) March 2011, and (c) April 2011. (unit: meter)

In general, frequencies change spatially due to the contribution of a certain combination of frequencies that refer to the gravitational signal at each point on the Earth's surface and this spatial rise of the frequencies is not reflected in the spherical harmonics. Consequently, any local change of the gravity affects the whole table of spherical harmonic coefficients, so that it is difficult to isolate the earthquake anomalies from other signals in the frequency domain.

Fig. 7 presents the multiscale geoid models using the Abel-Poisson scale function and wavelets on individual points of a 0.1°×0.2° grid space.

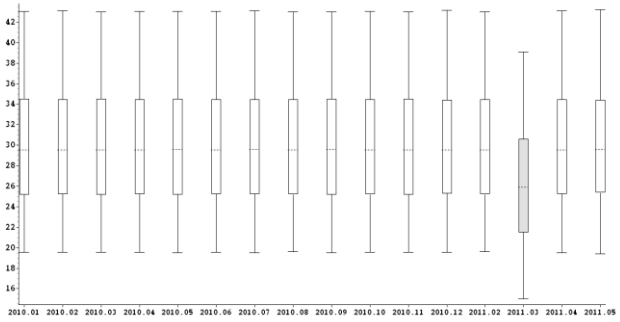

Fig. 8: Time-series of box plot with respect to multiscale geoid models for the period from January 2010 to May 2011. Mean of the geoid height for the whole period is 31.23148 m with range 10.28595~44.61724 m and standard deviation 8.19931 m. (unit: meter)

The researchers plot time-series box plots with respect to the multiscale geoid models and their changes from January 2010 to May 2011 in order to investigate whether or not those phenomena shown in Fig. 7 (b) are temporary. Figure 8 shows that the decrease of the multiscale geoid is an unexpected phenomenon that occurred in March 2011.

When Fig 7. is compared with Fig. 4, it can be seen that the multiscale geoid models are relatively underestimated on land but overestimated in the ocean as shown in Fig. 9. Also, it can be distinguished that multiscale geoid heights have decreased simultaneously in the order a few meters in Fig. 8 indicating that coseismic geoid changes associated with the Tohoku-Oki earthquake did occur. Note that the actual geoid changes the moment the earthquake occurred may be overestimated because monthly GRACE gravity data are produced by monthly average values before and after earthquake.

Figure 9 presents the difference between monthly geoid models and multiscale geoid models.

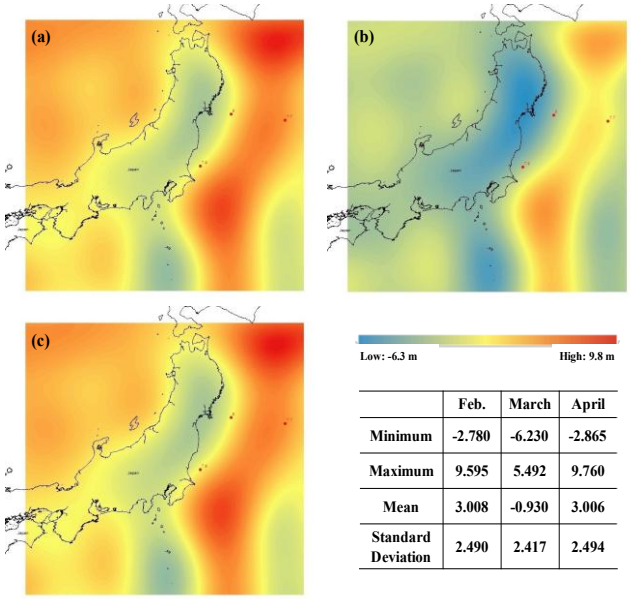

	Feb.	March	April
Minimum	-2.780	-6.230	-2.865
Maximum	9.595	5.492	9.760
Mean	3.008	-0.930	3.006
Standard Deviation	2.490	2.417	2.494

Fig. 9.: The difference between monthly geoid model and multiscale geoid model on individual points of a 0.1°×0.2° grid space for (a) February 2011, (b) March 2011, and (c) April 2011. (unit: meter)

3.2. Classification of the signal contribution

We divide up the long-wavelength and the medium-to-short-wavelength part to classify the signal contribution.

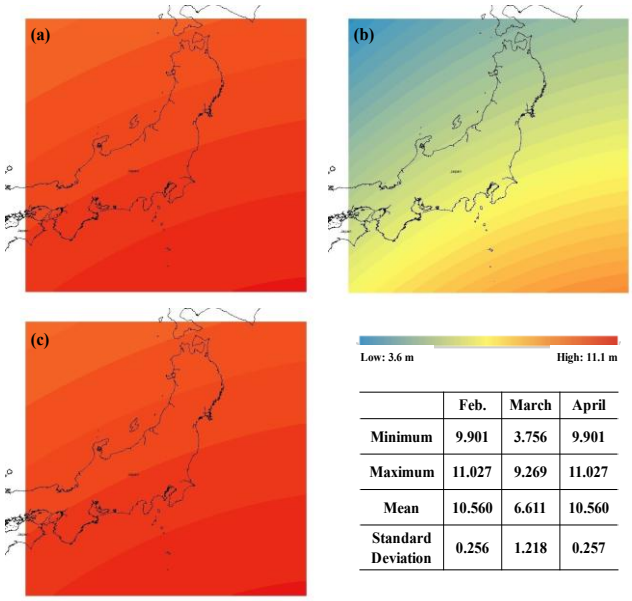

	Feb.	March	April
Minimum	9.901	3.756	9.901
Maximum	11.027	9.269	11.027
Mean	10.560	6.611	10.560
Standard Deviation	0.256	1.218	0.257

Fig. 10: Multiscale geoid models (at scale level 2) based on the GRACE gravity data in the long-wavelength part for (a) February 2011, (b), March 2011 and (c) April 2011. (unit: meter)

Figure 10 presents multiscale geoid models in the long-wavelength part. It can be seen that there is little geoid change in the long-wavelength part in February and April 2011, but there is a change in March 2011 when the Tohoku-Oki earthquake did occur. More details can be seen in Fig. 11 and Fig. 12.

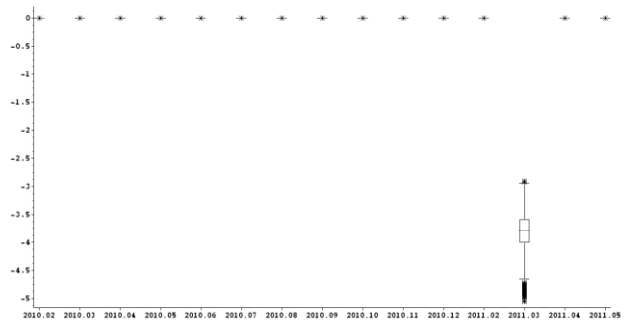

Fig. 11: Time-series of box plot with respect to the differences between the multiscale geoid models in the long-wavelength part for the period from February 2010 to May 2011 and that of January 2010 selected as the reference. (unit: meter)

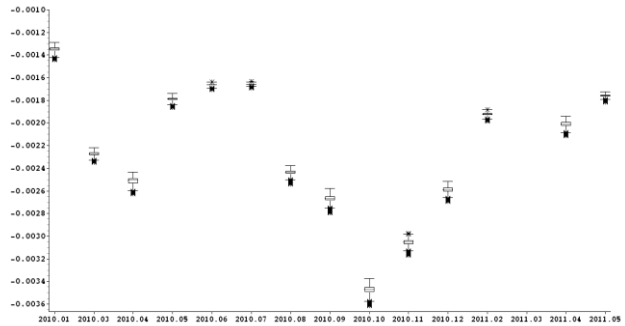

Fig. 12: Time-series of box plot with respect to the differences between the multiscale geoid models in the long-wavelength part for the period from February 2010 to May 2011 (except March 2011) and that of January 2010 selected as the reference (unit: meter). For comparison in the long-wavelength part, the multiscale geoid models from February 2010 to May 2011 are differenced with that of January 2010 selected as the reference. As shown in Fig.11, the multiscale geoid heights decreased with range -6.10127~-1.70579 m, mean -3.94599 m, and standard deviation 0.96578 m between February and March 2011. It is also notable that the geoid changes between February 2010 and March 2011 with range -6.08092~-1.71930 m, mean -3.94977 m, and standard deviation 0.96879 m showed a decrease in the amount of similar decreases as the change between February and March 2011. According to Park and Hong [37], a multiscale geoid height in March 2011 decreased simultaneously in the order of a few meters on average throughout the studied area, indicating that a coseismic geoid change induced by the Tohoku-Oki earthquake did occur. They also argued that this phenomenon was mainly due to seawater redistribution or ocean currents caused by the earthquake-triggered tsunami since it could be clearly seen in the long-wavelength part, not in the medium-to-short-wavelength one. Figure 13 presents multiscale geoid models in the medium-to-short-wavelength part. Unlike Fig. 10, it can be seen that there is not only little change in the geoid model over all periods but also no earthquake-induced signals associated with the Tohoku-Oki earthquake.For a more detailed comparison in the medium-to-short-wavelength part, the multiscale geoid models from February 2010 to May 2011 are compared with that of January 2010 selected as the reference.

As shown in Fig.14, there are changes showing the small differences in the order of a few centimeters in terms of center, spread and range of each geoid model., but it can be seen that these changes do not actually deviate significantly from January 2010. Note that these changes of the geoid models include both the temporal and the coseismic variations due to redistribution of masses at shorter time and spatial scales.

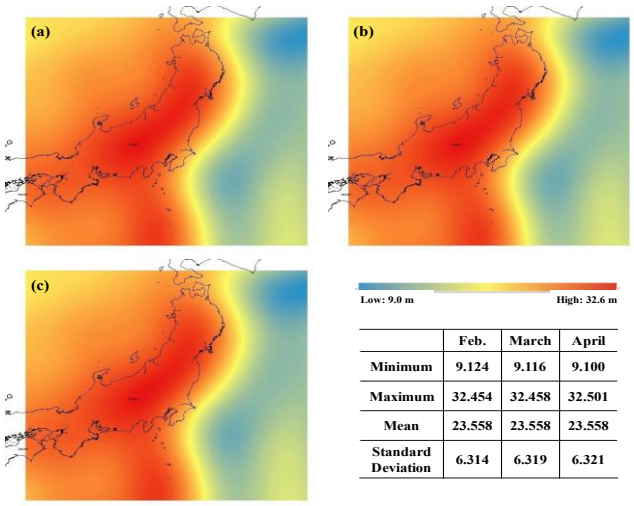

	Feb.	March	April
Minimum	9.124	9.116	9.100
Maximum	32.454	32.458	32.501
Mean	23.558	23.558	23.558
Standard Deviation	6.314	6.319	6.321

Fig. 13: Multiscale geoid models (adding up the scale levels from 2 to 7) based on the GRACE gravity data in the medium-to-short-wavelength part for (a) February 2011, (b), March 2011 and (c) April 2011. (unit: meter)

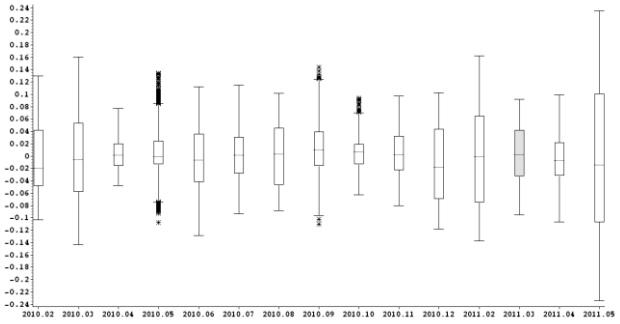

Fig. 14: Time-series of box plot with respect to the differences between the multiscale geoid models in the medium-to-short-wavelength part for the period from February 2010 to May 2011 and that of January 2010 selected as the reference (unit: meter).

3.3. Identification of the earthquake-induced signals

In order to find out more specific earthquake-related signals causing the decrease of the geoid height in the medium-to-short-wavelength part, each multiscale geoid model excluding the signals in the long-wavelength part from February 2010 to March 2012 is compared with that of January 2010 selected as the reference. Then it is plotted in conjunction with spatial location to analyze where geoid changes in the long-wavelength part are most prominent as shown in Fig. 15.

As shown in Fig. 15 (a), geoid heights have consistently increased at both at the northwestern part of the Yamagata Prefecture (hereafter denoted by a letter A) and at the southern part of the Sanriku segment near the Japan Trench (hereafter denoted by a letter C) until February 2011, while they have decreased consistently at the eastern part of northern Honshu near the Miyagi segment (hereafter denoted by a letter B) until February 2011 as of January 2010. Thereafter, the geoid change at A is suddenly reversed in March 2011 shown in Fig. 15 (b). With regard to the changes at both B and C, those decreasing and increasing tendencies are ongoing until July 2011, and are finally switched in August 2011 as shown in Fig. 15 (c).

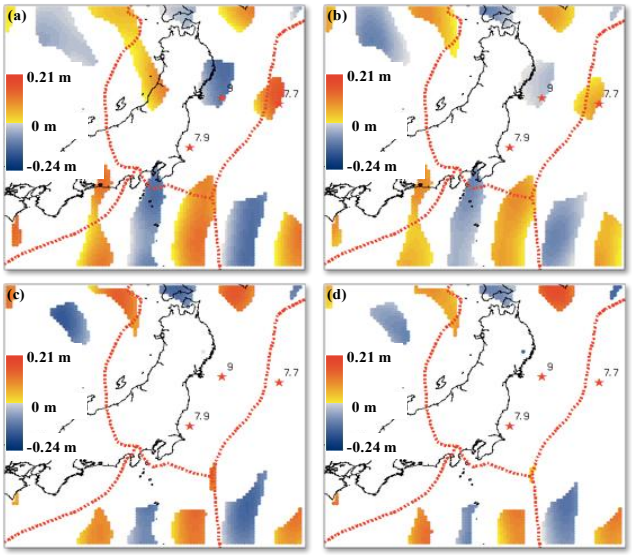

Fig. 15: Changes in the multiscale geoid models in the medium-to-short-wavelength part (unit: meter). Each geoid model in the subplots is differenced with that of January 2010 selected as the reference. (a) changes observed in February 2011 (before the earthquake), (b) changes observed in March 2011 (after the earthquake), (c) changes observed in August 2011 and (d) changes observed in March 2012.

No signals associated with the 2011 Tohoku-Oki earthquake were detected when the same analysis was performed on each geoid model with February 2010 to February 2011 as the reference instead of January 2010. Thus, it can be inferred that not only is there a pattern where the increasing geoid height at A has been ongoing since at least January 2010, but also that this phenomenon plays a very important role in the occurrence of the Tohoku-Oki earthquake.

Figure 16 shows the coseismic and postseismic geoid changes. As shown in Fig. 16 (b), the changes at A, B and C started to stand out in December 2010 when compared with those from the previous months. In March 2011, a significant geoid decrease is found at A by changing its positive domain into a negative one (dashed circle in Fig. 16 (d)). This transition may result from the mass redistribution mainly due to the seafloor subsidence or crust dilatation caused by the Tohoku-Oki earthquake. Note that the changes at both B and C keep up with their changing patterns and remain in each domain, although the geoid models come close to those of the reference, which reflects that the earthquake energy is not fully released until at least March 2011.

As shown in Fig. 16 (e), the change in May 2011 shows the largest one throughout the study, which may be a result of releasing the earthquake energy that has remained after the Tohoku-Oki earthquake. In August 2011, significant geoid changes occur not only by changing their domains at B and C into positive and negative ones (solid circles in Fig.

16 (g)), respectively, but also by changing its positive domain into a negative one (dashed circle in Fig. 16 (g)) at the southeastern part of A that was restored again after the earthquake.

Figure 17 shows the geoid changes at A, B and C in the time-series box plots. As shown in Fig. 17 (a), the range of the change in December 2010 is expanded with a minimum of -0.119 m, a maximum of 0.108 m, a mean of 0.022 m and a standard deviation of 0.088 m. This data looks very similar to the data from June 2010, ranging from -0.129 to 0.112 m, with a mean of 0.014 m and a standard deviation of 0.088 m. If this is a common or periodic phenomenon, it is anticipated that the change for February 2011 will be similar or limited. However, it becomes more widespread, ranging from -0.138 to 0.163 m, with a mean of 0.012 m and a standard deviation of 0.093 m. In March 2011, the spread distribution suddenly narrows with a minimum of -0.026 m, a maximum of 0 m, a mean of 0.014 m and a standard deviation of 0.008 m. Note that the values under the upper quartile correspond with those at both A and B as shown in Fig. 17 (b) and Fig. 17 (c). Meanwhile, the change at A shown in Fig. 17 (b) shows a slightly different pattern compared with that of C shown in Fig. 17 (d) although those are included in the same positive domain. For example, the changes between July and August 2010 move in an opposite direction (dashed circles in Fig. 17 (b) and Fig. 17 (d)). Also, the change at A begins to decrease in February 2011 and turns the positive domain into a negative one in March 2011, while the change at C still keeps the positive domain even though the changes at both A and C show the same pattern of decrease between February and March 2011 (solid circles in Fig. 17 (b) and Fig. 17 (d)). Thus, it can be inferred that the geological relationship between A and B as well as those changing patterns may immediately affect the Tohoku-Oki earthquake occurrence.

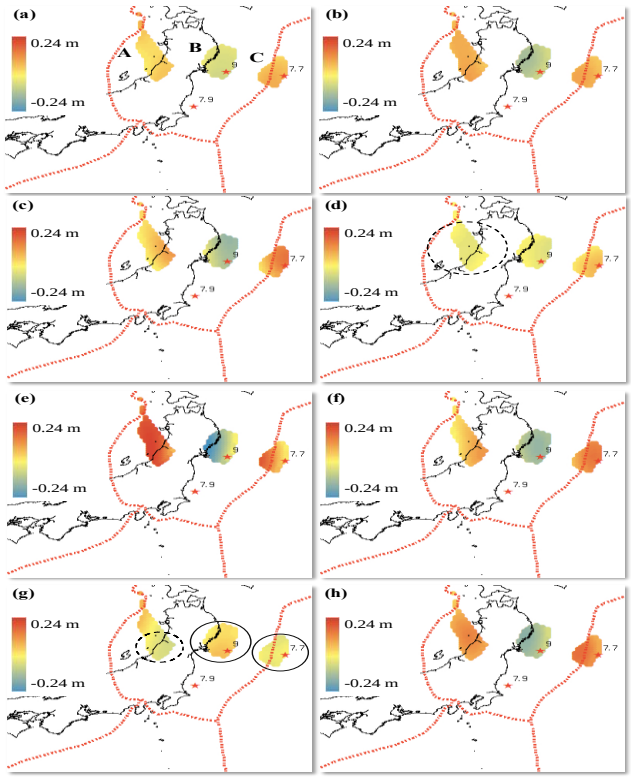

Fig. 16: Changes in the multiscale geoid models in units of meter at the northwestern part of the Yamagata Prefecture (denoted by a letter A), the southern part of the Sanriku segment near the Japan Trench (denoted by a letter C) and the eastern part of northern Honshu near the Miyagi segment (denoted by a letter B) in (a) February 2010, (b) December 2010, (c) February 2011, (d) March 2011, (e) May 2011, (f) July 2011, (g) August 2011 and (h) March 2012. The geoid height at A has consistently increased until February 2011 as of January 2010, and became completely or partially extinct in March (dashed circle in Fig. 16 (d)) and August 2011 (dashed circle in Fig. 16 (g)). The geoid anomalies at B and C have consistently decreased and increased until July 2011 as of January 2010, respectively, and are completely reversed in August 2011 (solid circles in Fig. 16 (g)).The range of the changes in May 2011 is very wide, with a minimum of -0.235 m, a maximum of 0.239 m, a mean of 0.06 m and a standard deviation of 0.158 m. Also, it is the largest one shown in Fig. 17 (a). Additionally, when comparing the maximum and minimum values throughout the studied area presented in Park and Hong [37] with those at A, B, and C, shown in Fig. 17 (a), it can be found that the changes at these regions are in control of this phenomenon. Thus, it is assumed that the mass redistribution caused by the Tohoku-Oki earthquake has made more intense progress not just after the earthquake but in May 2011.

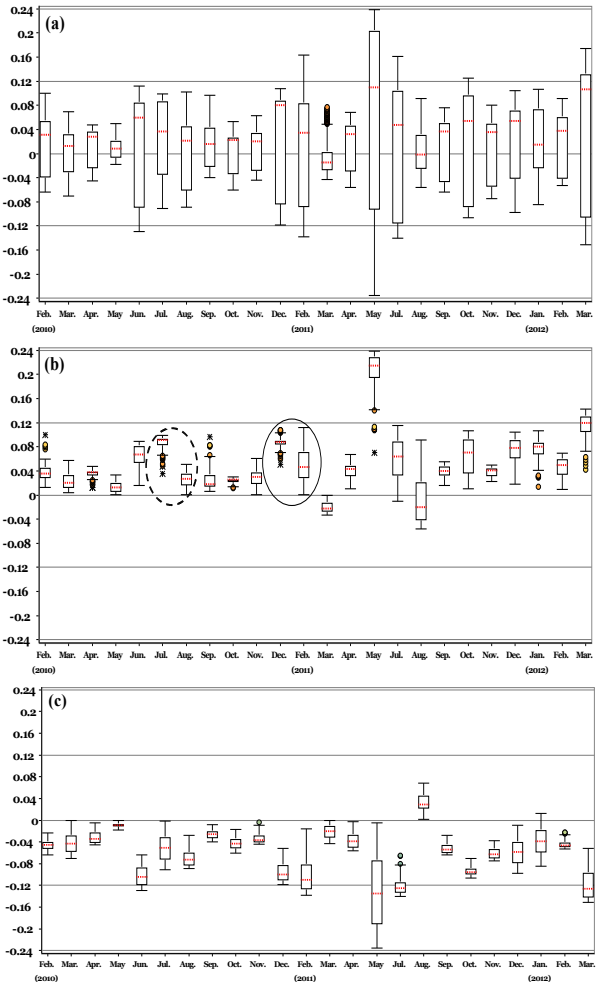

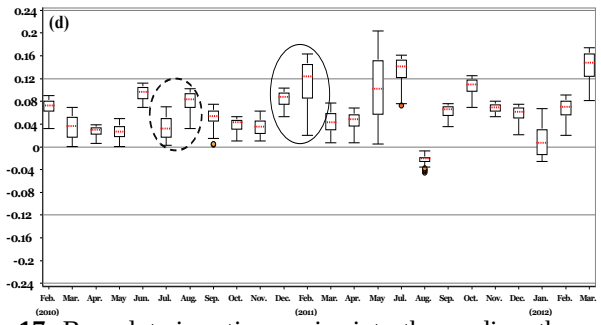

Fig. 17: Box plots in a time-series into the median, the upper and lower quartiles, and the minimum and maximum values showing center, spread, range, and any outliers in units of meter (a) Changes in the geoid anomalies for A, B and C (denoted in Fig. 16 (a)) between February 2010 and March 2012. (b) Same as Fig. 17 (a), but corresponding to those for A. (c) Same as Fig. 17 (a), but correspond to those for B. (d) Same as Fig. 17 (a), but corresponding to those for C. (unit: meter)

When Fig. 17 (a) is seen in greater detail, it becomes clear that the change in July 2011 is very similar to that of February 2011. Actually, the changes in each following month (i.e. March and August 2011, respectively) show a similar pattern as well. However, there is a feature that does not specifically identify with the pattern shown in Fig. 17 (a). In other words, the change at A shown in Fig. 17 (b) is especially predominant in March 2011, but the changes at both B and C shown in Fig. 17 (c) and Fig. 17 (d) are especially predominant in August 2011. Also, it is obvious that the changing patterns in the geoid anomalies at both B and C look very similar, but are opposite in direction throughout the study, just like they were reflected into a mirror. Thus, it can be inferred that the geological relationship between B and C, as well as those changing patterns, may also play a very important role in the Tohoku-Oki earthquake occurrence.

The range of the changes in August 2011 becomes narrow, showing a similar spread distribution with a minimum of -0.023 m, a maximum of 0.03 m, a mean of 0.001 m and a standard deviation of 0.019 m compared to the data from March 2011. However, there is a significant difference between them. For example, the values in the spread are not only included in both the positive and negative domains in and around the reference, but they also mainly correspond with those at both B and C, as well as a portion of those at A shown in Fig. 17 (b), Fig. 17 (c) and Fig. 17 (d). Thus, it can be assumed that the geological relationship among A, B and C may affect the Tohoku-Oki earthquake occurrence by interacting with one another.

IV. CONCLUSION

In general, great subduction earthquakes such as the 2004 Sumatra-Andaman islands and the 2010 Maule, Chile induced larger, sustained negative gravity change on land and smaller positive gravity changes offshore [8], [20], [21], [22], [38], [39]. This is the characteristic spatial pattern of a coseismic gravity change after undersea thrust earthquakes accompanied by crustal dilatation. In the medium-to-short-wavelength part, coseismic and postseismic geoid changes were detected at the northwestern part of the Yamagata Prefecture, the southern part of the Sanriku segment near the Japan Trench and the eastern part of northern Honshu near the Miyagi segment. Geoid heights consistently increased at the first two regions and decreased at the last one until February 2011. In March 2011, a significant decrease was found at the northwestern part of the Yamagata Prefecture. This is in agreement with the findings of [38], [39], [40] and [41]. This transition might be a result of the mass redistribution caused by the Tohoku-Oki earthquake. However, the changes at the rest of the regions were still in existence and maintained their patterns of decreasing and increasing in each domain, respectively.With regard to the postseismic recovery of the geoid, the changes in the eastern part of northern Honshu near the Miyagi segment and the southern part of the Sanriku segment near the Japan Trench were especially predominant in August 2011. The spatial pattern is in agreement with the results of Han et al. [39]. Eventually, the geological relationship among the northwestern part of the Yamagata Prefecture, the southern part of the Sanriku segment near the Japan Trench and the eastern part of northern Honshu near the Miyagi segment played a very important role in the Tohoku-Oki earthquake occurrence by interacting with one another.With the assumption that this feature is related to the earthquake energy release triggered by the Tohoku-Oki earthquake, it can be concluded that the balance of energy among the northwestern part of the Yamagata Prefecture, the southern part of the Sanriku segment near the Japan Trench and the eastern part of northern Honshu near the Miyagi segment, which had been maintained until February 2011, was broken between the northwestern part of the Yamagata Prefecture and the eastern part of northern Honshu near the Miyagi segment before the earthquake.The earthquake energy which still remained was released between the eastern part of northern Honshu near the Miyagi segment and the southern part of the Sanriku segment near the Japan Trench in August, 2011. Thus, it can be deduced that the tectonic plate motion around the Japanese islands may reach a period of geological stability after August 2011. However, any signal associated with the magnitude 7.7 aftershock that occurred at the southwestern part of the epicenter could not be found in this analysis. Therefore, it can be inferred that this aftershock might be a result of other causes such as the imbalance of the energy between the North American plate and the Philippine Sea plate, triggered by the Tohoku-Oki earthquake. To better understand the geodynamic process between the Tohoku-Oki earthquake and its aftershocks, it is necessary to carry out further studies.

Acknowledgement

The authors would like to thank the German Space Operations Center (GSOC) of the German Aerospace Center (DLR) for providing continuously and nearly 100% of the raw telemetry data of the twin GRACE satellites.

REFERENCES

1. DeMets C, Gordon RG, Argus DF & Stein S (1990), Current plate motions. *Geophysical Journal International* 101, 425–478.
2. Simons M, Minson SE, Sladen A, Ortega F, Jiang J, Owen SE, Meng L, Ampuero JP, Wei S, Chu R, Helmberger DV, Kanamori H, Hetland E, Moore AW & Webb FH (2011), The 2011 Magnitude 9.0 Tohoku-Oki Earthquake: Mosaicking the Megathrust from Seconds to Centuries. *Science* 332, 1421–1425.

3. Minoura K, Imamura F, Sugawara D & Kono Y (2001), The 869 Jögan tsunami deposit and recurrence interval of large-scale tsunami on the Pacific coast of northeast Japan. *Journal of Natural Disaster Science* 23, 83–88.
4. Dickey JO, Bentley CR, Bilham R, Carton JA, Eanes RJ, Herring TA, Kaula WM, Lagerloef GSE, Rojstaczer S & Smith WHF (1998), Satellite gravity: insights into the solid earth and its fluid envelope. *Eos, Transactions American Geophysical Union* 79, 237–243.
5. Broerse DBT, Vermeersen LLA, Riva REM & van der Wal W (2011), Ocean contribution to co-seismic crustal deformation and geoid anomalies: Application to the 2004 December 26 Sumatra–Andaman earthquake. *Earth and Planetary Science Letters* 305, 341–349.
6. Tapley BD, Bettadpur S, Ries JC, Thompson PF & Watkins MM (2004), GRACE measurements of mass variability in the Earth system. *Science* 305, 503–505.
7. Chambers DP (2006), Evaluation of new GRACE time-variable gravity data over the ocean. *Geophysical Research Letters* 33, L17603.
8. Han SC, Shum CK, Ries JC, Bevis M, Ji C & Kuo CY (2006), Crustal dilatation observed by GRACE after the 2004 Sumatra-Andaman earthquake. *Science* 313, 658–662.
9. Davis JL, Tamisiea ME, Elósegui P, Mitrovica JX & Hill EM (2008), A statistical filtering approach for Gravity Recovery and Climate Experiment (GRACE) gravity data. *Journal of Geophysical Research* 113, B04410.
10. Han SC, Shum CK, Jekeli C, Kuo CY, Wilson C & Seo KW (2005), Non-isotropic filtering of GRACE temporal gravity for geophysical signal enhancement. *Geophysical Journal International* 163, 18–25.
11. Chen JL, Wilson CR & Seo KW (2006), Optimized smoothing of Gravity Recovery and Climate Experiment (GRACE) time-variable gravity observations. *Journal of Geophysical Research* 111, B06408.
12. Swenson S & Wahr J (2006), Post-processing removal of correlated errors in GRACE data. *Geophysical Research Letters* 33, L08402.
13. Sasgen I, Martinec Z & Fleming K (2006), Wiener optimal filtering of GRACE data. *Studia Geophysica et Geodaetica* 50, 499–508.
14. Zhang ZZ, Chao BF, Lu Y & Hsu HT (2009), An effective filtering for GRACE time-variable gravity: Fan filter. *Geophysical Research Letters* 36, L17311–6.
15. Fengler MJ, Freeden W, Kohlhaas A, Michel V & Peters T (2007), Wavelet modeling of regional and temporal variations of the earth's gravitational potential observed by GRACE. *Journal of Geodesy* 81, 5–15.
16. Chen JL, Wilson CR, Tapley BD & Grand S (2007), GRACE detects coseismic and postseismic deformation from the Sumatra-Andaman earthquake. *Geophysical Research Letters* 34, L13302.
17. Imanishi Y, Sato T, Higashi T, Sun W & Okubo S (2004), A Network of Superconducting Gravimeters Detects Submicrogal Coseismic Gravity Changes. *Science* 306, 476-478.
18. Sun W & Okubo S (2004), Coseismic deformations detectable by satellite gravity missions—A case study of Alaska (1964, 2002) and Hokkaido (2003) earthquakes in the spectral domain. *Journal of Geophysical Research* 109, B04405.
19. Panet I, Mikhailov V, Diament M, Pollitz FF, King G, de Viron O, Holschneider M, Biancale R & Lemoine JM (2007), Coseismic and post-seismic signatures of the Sumatra 2004 December and 2005 March earthquakes in GRACE satellite gravity. *Geophysical Journal International* 171, 177-190.
20. De Linage C, Rivera L, Hinderer J, Boy JP, Rogister Y, Lambotte S & Biancale R (2009), Separation of coseismic and postseismic gravity changes for the 2004 Sumatran earthquake from 4.6 yr of GRACE observations and modelling of the coseismic change by normal mode summation. *Geophysical Journal International* 176, 695–714.
21. Han SC, Sauber J & Luthcke S (2010), Regional gravity decrease after the 2010 Maule (Chile) earthquake indicates large-scale mass redistribution. *Geophysical Research Letters* 37, L23307.
22. Heki K & Matsuo K (2010), Coseismic gravity changes of the 2010 earthquake in Central Chile from satellite gravimetry, *Geophysical Research Letters* 37, L24306.
23. Freeden W & Schneider F (1998), Wavelet approximations on closed surfaces and their application to boundary-value problems of potential theory. *Mathematical methods in the applied sciences* 21, 129–163.
24. Freeden W & Michel V (1999), Constructive approximation and numerical methods in geodetic research today–an attempt at a categorization based on an uncertainty principle, *Journal of Geodesy* 73, 452–465.
25. Freeden W, Glockner O & Thalhammer M (1999), Multiscale gravitational field recovery from GPS-satellite-to-satellite tracking, *Studia Geophysica et Geodaetica* 43, 229–264.
26. Hofmann-Wellenhof B & Moritz H, *Physical Geodesy*, Springer Science & Business Media, (2005), pp:59–64.
27. Freeden W & Windheuser U (1996), Spherical Wavelet Transform and its Discretization. *Advances in Computational Mathematics* 5, 51–94.
28. Freeden W & Windheuser U (1997), Combined spherical harmonic and wavelet expansion – a future concept in Earth's gravitational determination. *Applied and Computational Harmonic Analysis* 4, 1–37.
29. Freeden W & Schreiner M (2005), Spaceborne gravitational field determination by means of locally supported wavelets. *Journal of Geodesy* 79, 431–446.
30. Freeden W & Schreiner M (2006), Local Multiscale Modelling of geoid undulations from deflections of the vertical. *Journal of Geodesy* 79, 641–645.
31. Freeden W & Schreiner M (2007), Biorthogonal Locally Supported Wavelets on the Sphere Based on Zonal Kernel Functions. *Journal of Fourier Analysis and Applications* 13, 693–709.
32. Freeden W & Michel V, *Multiscale Potential Theory with Applications to Geoscience*, Birkhäuser Basel, (2004).
33. Dahlke S, Dahmen W, Schmitt E & Weinreich I (1995), Multiresolution Analysis and Wavelets on S^2 and S^3. *Numerical Functional Analysis and Optimization* 16, 19–41.
34. Freeden W & Schneider F (1998), An integrated wavelet concept of physical geodesy. *Journal of Geodesy* 72, 259–281.
35. Driscoll JR & Healy DM (1994), Computing Fourier Transforms and Convolutions on the 2-Sphere. Advances in Applied Mathematics 15, 202–250.
36. Freeden W, Gervens T & Schreiner M, *Constructive approximation on the Sphere*, Oxford Science Publications, (1998).
37. Park SH & Hong SW (2018), Identifying Seismic Geoid Changes of the 2011 Tohoku-Oki Earthquake in the Medium-to-Short Wavelength Part. *Asia-Pacific Advanced Research in Electrical and Electronics Engineering* 2, 9–14.
38. Matsuo K & Heki K (2011), Coseismic gravity changes of the 2011 Tohoku-Oki earthquake from satellite gravimetry. *Geophysical Research Letters* 38, L00G12.
39. Han SC, Sauber J & Riva REM (2011), Contribution of satellite gravimetry to understanding seismic source processes of the 2011 Tohoku-Oki earthquake, *Geophysical Research Letters* 38, L24312.
40. Wang L, Shum CK, Simons FJ, Tapley BD & Dai C (2012), Coseismic and postseismic deformation of the 2011 Tohoku-Oki earthquake constrained by GRACE gravimetry, *Geophysical Research Letters* 39, L07301.
41. Zhou X, Sun W, Zhao B, Fu G, Dong J & Nie Z (2012), Geodetic observations detecting coseismic displacements and gravity changes caused by the Mw = 9.0 Tohoku-Oki earthquake, *Journal of Geophysical Research* 117, B05408.
42. Kirby J & Featherstone W, A study of zero- and first-degree terms in geopotential models over Australia, Geomatics Research Australia 66, 93–108.